J. Fluid Mech. (1995), *vol.* 285, *pp.* 95–122

Two-dimensional periodic waves in shallow water. Part 2. Asymmetric waves

By JOE HAMMACK[1], DARYL McCALLISTER[2], NORMAN SCHEFFNER[3] AND HARVEY SEGUR[2]

[1] Departments of Geosciences and Mathematics, Penn State University, University Park, PA 16802, USA

[2] Program in Applied Mathematics, University of Colorado, Boulder, CO 80309-0526, USA

[3] US Army Engineer Waterways Experiment Station, Coastal Engineering Research Center, Vicksburg, MS 39180, USA

(Received 8 October 1993 and in revised form 13 September 1994)

We demonstrate experimentally the existence of a family of gravity-induced finite-amplitude water waves that propagate practically without change of form in shallow water of uniform depth. The surface patterns of these waves are genuinely two-dimensional, and periodic. The basic template of a wave is hexagonal, but it need not be symmetric about the direction of propagation, as required in our previous studies (e.g. Hammack *et al.* 1989). Like the symmetric waves in earlier studies, the asymmetric waves studied here are easy to generate, they seem to be stable to perturbations, and their amplitudes need not be small. The Kadomtsev–Petviashvili (KP) equation is known to describe approximately the evolution of waves in shallow water, and an eight-parameter family of exact solutions of this equation ought to describe almost all spatially periodic waves of permanent form. We present an algorithm to obtain the eight parameters from wave-gauge measurements. The resulting KP solutions are observed to describe the measured waves with reasonable accuracy, even outside the putative range of validity of the KP model.

1. Introduction

An earlier paper by Hammack, Scheffner & Segur (1989, hereinafter called Part 1) reported an experimental study of gravity-induced waves that propagate practically without change of form in shallow water of uniform depth. Those waves had finite amplitudes, and their surface patterns were periodic in two spatial dimensions and in time. The spatial pattern of the waves was a hexagon that was symmetric about the direction of wave propagation. The waves were predicted with reasonable accuracy by a family of exact solutions of an equation due to Kadomtsev & Petviashvili (1970) known as the KP equation:

$$(f_t + 6ff_x + f_{xxx})_x + 3f_{yy} = 0,$$

where subscripts denote partial derivatives. In a second set of experiments (Hammack, Scheffner & Segur 1991), more effort was made to reduce depth variations in the laboratory basin, and the theoretical–experimental agreement improved further. Both of these studies were preceded by Peregrine (1985), who also observed hexagon-like waves of permanent form but who argued against that interpretation.

Within the KP equation, almost all real-valued spatially periodic waves of permanent form are characterized by a family of exact solutions with eight free parameters: six

dynamic parameters associated with wavelengths and wave amplitudes, plus two arbitrary phases (cf. Segur & Finkel 1985). Typically, these waves have asymmetric surface patterns. The two experimental papers cited above tested only a subset of these waves, called *symmetric* waves, which have only (3+2) parameters. Figure 1 shows photographs of both symmetric and asymmetric water waves.

In this paper, we describe an experimental study of two-dimensional spatially periodic *asymmetric* waves that propagate practically without change of form in shallow water of uniform depth. (In the terminology used in this paper, surface waves are either 'one-dimensional' or 'two-dimensional', depending on the nature of their surface patterns. The velocity fields associated with the waves are one dimension higher.) Our three main results for asymmetric waves are consistent with our earlier results for symmetric waves:

(i) In shallow water of uniform depth, there exist spatially periodic waves with finite amplitudes and fully two-dimensional surface patterns. These waves are easy to generate, they propagate with nearly permanent form, and they seem to be stable with respect to perturbations in initial conditions and to weak external forcing (e.g. due to viscosity or to variations in bottom depth). The amplitudes of the waves need not be small.

(ii) The basic template of the two-dimensional wave pattern is a six-sided figure (i.e. a hexagon), with a broad, flat trough surrounded by six narrow wave crests (see figure 1). Wave crests opposite each other in this hexagon are parallel, they are equal in length and in wave amplitude, and they can be identified with each other in order to reproduce the periodic pattern.

(iii) Over the range of parameter values that we tested, these water waves are predicted with reasonable accuracy by the full eight-parameter family of KP solutions of genus 2. This range extends well beyond the putative range of validity of the KP equation as an approximate model of waves in shallow water (i.e. beyond the range of nearly one-dimensional waves of small amplitude in shallow water). In this sense, the KP model provides a convenient means to learn about hexagonal waves of permanent form, but their mathematical existence and stability seem to be independent of the KP model.

Our primary objective in this study is to establish experimentally the existence and properties of asymmetric hexagonal waves of permanent form in shallow water of uniform depth. To this end, we present the results of fifteen experiments, which exhibit some of the variety of waves of this form. Our secondary objective is to determine how accurately the full eight-parameter family of KP solutions of genus 2 describe the measured waves. To this end, we present an algorithm that uses measurements from an array of wave gauges to obtain the eight parameters of the KP solution that 'best' fit the measured waves. By design, the algorithm uses only wave-gauge measurements (ignoring the known data used to program the wavemaker) so that it can be applied to gauge-array data in more complex wave environments in the laboratory and in the field. Fifteen experiments are far too few to determine the parameter range for KP theory to be applicable, and our experiments were not chosen with that objective in mind. In fact, most of our experiments have parameters that lie outside the putative range of validity of KP theory. (Some of our waves have near-breaking heights and strongly two-dimensional surface patterns.) We reiterate our belief that the KP model is convenient but not essential to describe periodic waves of permanent form in shallow water.

A summary of the contents of this paper is as follows. In §2, we review the main ideas needed to compare KP solutions of genus 2 with experimental data on waves in shallow

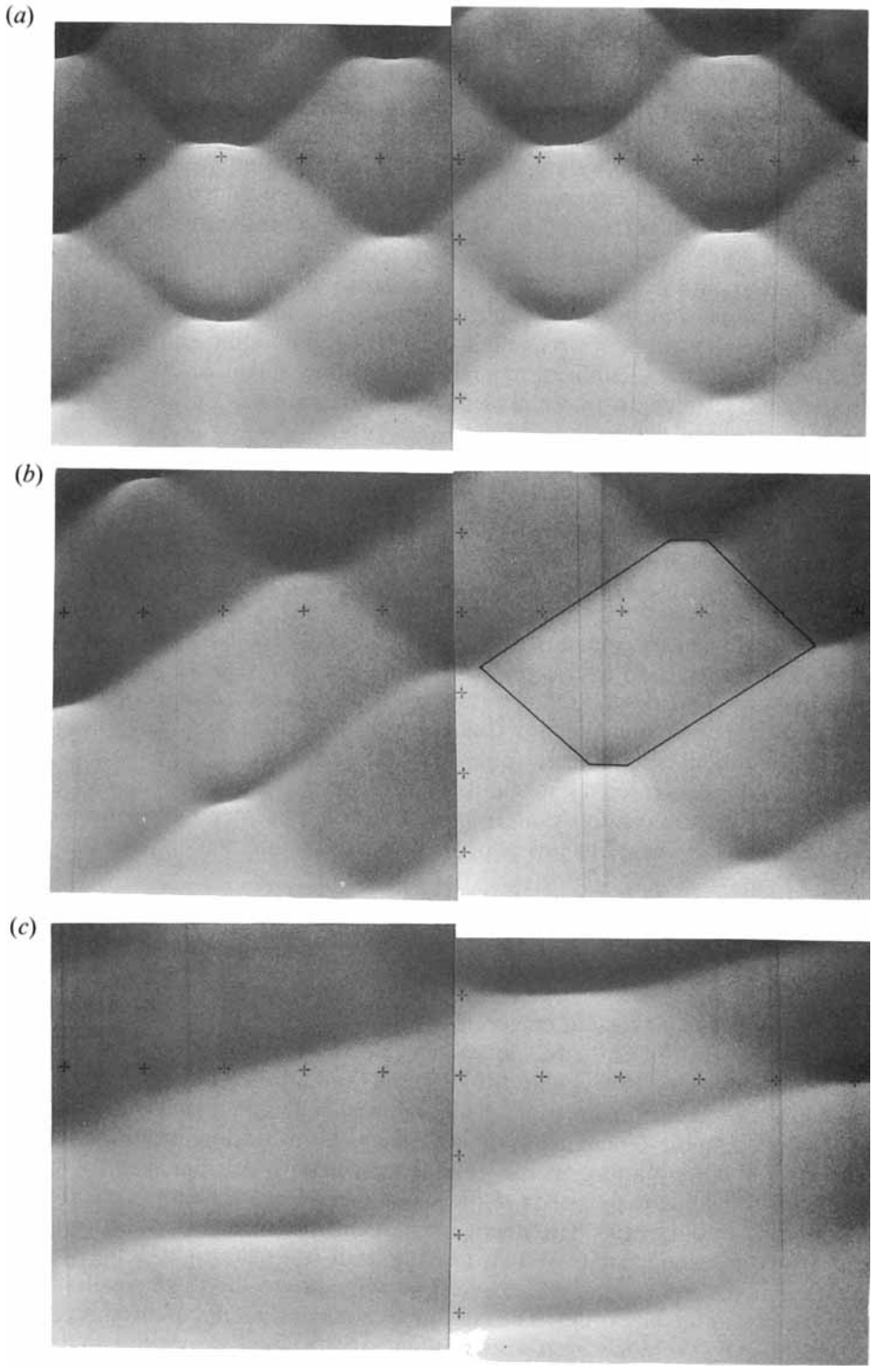

FIGURE 1. Mosaic of two overhead photographs, showing surface patterns of waves in shallow water. Experiment: (*a*) KP38.50204; (*b*) KP400203-300303; (*c*) KP220203-110403. Each of these wave patterns has a basic hexagonal template; one such hexagon is drawn in figure 1(*b*).

water. We describe experimental procedures and results in §3. The procedures are similar to those used in Part 1, but the experimental data here are more complicated. The main theoretical problem addressed in this paper is the following. Given wave-gauge data from a particular experiment, find the eight parameters of the KP solution of genus 2 that best fit these data. We present an algorithm to solve this problem in an Appendix to the paper, and we use the algorithm in §4 to compare KP theory with the results of fifteen different experiments. In a sense, our procedure can be viewed as a complicated form of surface-fitting (i.e. two-dimensional curve fitting), with no demonstrated predictive power. However, we recorded more data than we used to find the KP solution, and in §4 we also test the accuracy of some concrete predictions of the theory. The hexagonal waves studied in this paper and in Part 1 seem to be the simplest non-trivial waves of permanent form that are periodic and two-dimensional in shallow water. This identification suggests that they ought to occur frequently in natural oceanic settings. In §5, we present some observations of oceanic waves similar to those discussed in this paper.

2. Review of KP theory

The KP equation,

$$(f_t + 6ff_x + f_{xxx})_x + 3f_{yy} = 0,$$

describes approximately the slow evolution of gravity-induced waves on water of uniform depth when the waves are assumed: (i) to have horizontal lengthscales much longer than the fluid depth (this assumption is also called 'shallow water'); (ii) to propagate primarily in one direction (the x-direction), with only weak variations in the transverse y-direction; and (iii) to have small-to-moderate amplitudes. The KP equation is not well-posed as it stands ($f \equiv 0$ and $f = t$ both solve KP, and they coincide at $t = 0$), and one must interpret $\{\partial_x^{-1}\}$ in order to integrate KP in time. All of the KP solutions discussed in this paper satisfy a constraint:

$$\oint f(x, y, t)\,\mathrm{d}x = 0, \tag{1}$$

and this constraint eliminates the ambiguity of interpreting $\{\partial_x^{-1}\}$. Ablowitz & Villarroel (1991) studied this and related constraints.

A detailed derivation of the KP equation can be found in Segur & Finkel (1985), or elsewhere. Briefly, one begins with Stokes' (1847) equations for surface waves on an inviscid incompressible fluid resting on a horizontal bed under a constant gravitational force, g. Imposing the three assumptions above yields at leading order the linear one-dimensional wave equation, whose solution consists of left-going and right-going waves, each travelling with speed $(gh)^{1/2}$, where h is the mean depth of the fluid. Each set of waves, of course, has permanent form at this order (i.e. for short times). Over longer times, in a coordinate system moving with (say) the right-going waves, one observes that the right-going waves evolve slowly, due to the three small effects that were neglected at leading order. The last three terms in the KP equation represent the effect on this slow evolution of (i) weak nonlinearity, (ii) weak dispersion, and (iii) weak two-dimensionality.

Let $\{X, Y, Z\}$ represent spatial coordinates in a fixed laboratory frame with Z vertical, let T be time, let $\eta(X, Y, T)$ measure the elevation of the fluid surface above its mean level, and let $\epsilon \ll 1$ be a formal small parameter related to the assumptions

above. The scaled variables in KP can be related to the laboratory coordinates as follows:

$$x = \frac{\epsilon^{1/2}(X-(gh)^{1/2}T)}{h}, \quad y = \frac{\epsilon Y}{h}, \quad t = \frac{\epsilon^{3/2}X}{6h}, \quad f = \frac{3\epsilon\eta}{2h} + O(\epsilon^2). \tag{2}$$

This change of coordinates can be performed in more than one way; the choice used here is slightly unconventional, and it differs from that in Part 1: ordinarily one sets $t = \epsilon^{3/2}(gh)^{1/2}T/6h$. Either choice leads to a KP equation, but the solution must be interpreted slightly differently in the two cases. The current choice is more natural for our experimental configuration, but the main motivation for this choice is that it simplifies the surface-fitting algorithm presented in Appendix B.

As noted above, the KP equation is an approximate model of water waves for $\epsilon \ll 1$. In order to compare with definite experiments, we set $\epsilon = 1$ in this paper. To justify this, we note that the KP equation is invariant under the scaling

$$x \to \alpha x, \quad y \to \alpha^2 y, \quad t \to \alpha^3 t, \quad f \to \alpha^{-2} f. \tag{3}$$

Applying this scaling to (2) without the $O(\epsilon^2)$ terms, with $\alpha^2 = \epsilon$, amounts to setting $\epsilon = 1$ there. As a consequence, some free parameters in the solutions described below must be small for the validity of the approximation.

Krichever (1977) showed that the KP equation admits a huge family of exact solutions in the form

$$f(x, y, t) = 2\,\partial_x^2 \ln \Theta, \tag{4}$$

where Θ is a Riemann theta function of genus N. Here N identifies the number of independent phases in the solution, and f is a quasi-periodic function of these N phases. (Recall that 'quasi-periodic' means that f is periodic in each of the N phases, if the other $N-1$ phases are held fixed.) In the simplest case, $N = 1$ and (4) reproduces the familiar cnoidal wave (e.g. Wiegel 1960). The solutions of interest in this paper have $N = 2$, and Θ is given by a double Fourier series:

$$\Theta(\phi_1, \phi_2; B) = \sum_{m=-\infty}^{\infty} \sum_{n=-\infty}^{\infty} \exp\left[\tfrac{1}{2}(m^2 b + 2mnb\lambda + n^2(b\lambda^2 + d)) + \mathrm{i}(m\phi_1 + n\phi_2)\right], \tag{5}$$

where the phases ϕ_1 and ϕ_2 are given by

$$\phi_j = \mu_j x + \nu_j y + \omega_j t + \Phi_j \quad (j = 1, 2), \tag{6}$$

$\{\Phi_1, \Phi_2\}$ are arbitrary phase constants, and the real-valued parameters $\{b, \lambda, d\}$, which define the elements of the Riemann matrix (see Segur & Finkel 1985), satisfy the following constraints:

$$-\infty < b < 0, \quad 0 < \lambda < 1, \quad -\infty < d \leqslant b(1-\lambda^2). \tag{7}$$

Actually, the constraint on λ can be tightened to $[0 < \lambda \leqslant \frac{1}{2}]$. Even so, we use (7) because it allows us to assume that $\mu_1/\mu_2 \geqslant 0$, which simplifies the algorithm in Appendix B. For solutions of genus 2, formal asymptotic validity of the KP model of water waves requires the limit $\{\mu_j \to 0$, with (ν_j/μ_j^2) and (ω_j/μ_j^3) finite$\}$. However, we will demonstrate reasonable agreement between theory and experiment even for values of $\{\mu_1, \mu_2\}$ that are not very small.

The eight free parameters of a real-valued KP solution of genus 2 are $\{b, \lambda, d, \mu_1, \mu_2, \nu_2; \Phi_1, \Phi_2\}$. As noted by Dubrovin (1981) and by Segur & Finkel (1985),

the parameters can be selected as follows: (i) choose $\{b, \lambda, d\}$ to satisfy (7); (ii) choose μ_2 as an arbitrary positive number, and ν_2 as an arbitrary real number; (ii) choose (μ_1/μ_2) so that a sixth-order polynomial in (μ_1/μ_2) is positive (the polynomial can be found in Dubrovin 1981 or in Segur & Finkel 1985); then the square root of the polynomial yields ν_1; (iv) once ν_1 is known, then ω_1 and ω_2 can be found explicitly in terms of $\{\mu_1, \mu_2\}$; (v) choose $\{\Phi_1, \Phi_2\}$ as arbitrary real numbers, but since they are phase constants, it is sufficient to permit only

$$0 \leqslant \Phi_j < 2\pi \quad (j = 1, 2).$$

Every such choice of parameters yields a KP solution of genus 2 that is real-valued, that is periodic in two spatial directions and in time, and that propagates without change in form. The velocity of propagation (in KP coordinates) is given by

$$\frac{\mathrm{d}x}{\mathrm{d}t} = \frac{\nu_1\omega_2 - \nu_2\omega_1}{\mu_1\nu_2 - \mu_2\nu_1}, \quad \frac{\mathrm{d}y}{\mathrm{d}t} = \frac{\mu_1\omega_2 - \mu_2\omega_1}{\mu_2\nu_1 - \mu_1\nu_2}. \tag{8}$$

We obtain KP solutions using a FORTRAN code named DELTA. The code is available to interested readers through an anonymous `ftp` site; see Appendix A for details.

Symmetric solutions of genus 2 are obtained by imposing three additional restrictions on these parameters:

$$d = b(1-\lambda^2), \quad (\mu_1/\mu_2) = 1, \quad \nu_2 = -\nu_1. \tag{9}$$

It follows from these that $\omega_2 = \omega_1$, and that the KP solution is invariant under the transformation $\{y \to -y,\ x \to x,\ t \to t\}$. Among the KP solutions of genus 2, symmetric waves are special in at least three ways: (i) a symmetric wave propagates purely in the x-direction, because $\mathrm{d}y/\mathrm{d}t = 0$ in (8); (ii) a symmetric wave is specified by only $\{3+2\}$ free parameters, instead of by $\{6+2\}$, because of (9); and (iii) a symmetric wave is periodic in the x- and y-directions.

Symmetric solutions were the main focus of the work in Part 1, but not here.

3. Experimental programme and typical results

The experimental programme was similar to that described in Part 1 and identical to that described briefly in Hammack *et al.* (1991). Experiments were performed at the Coastal Engineering Research Center (CERC), US Army Engineer Waterways Experiment Station, Vicksburg MS. We used a basin, whose planform is shown schematically in figure 2, that comprised a uniform-depth section 12.55 m long and 26.52 m wide, and a section with a gently sloping (1:30) beach that absorbed most of the incident wave energy. In the uniform-depth section, the still water depth was 20 cm $\pm$ 3 mm.

A segmented wavemaker with 58 piston-type paddles, each 45.7 cm wide, spanned the wide wall opposite the beach. The wavemaker is described in detail by Scheffner (1988), and the wavemaker motion is described in Part 1. Briefly, the wavemaker was programmed to generate a superposition of two cnoidal wavetrains with different directions of propagation. In the current experiments, we allowed the wavelengths and/or amplitudes of the two cnoidal waves to differ, so that the resulting two-dimensional wave patterns would be asymmetric. The nomenclature of our experiments, e.g. KPaabbcc-AABBCC, is based on programming parameters for the wavemaker. The aa and AA represent the phase lags in degrees between adjacent

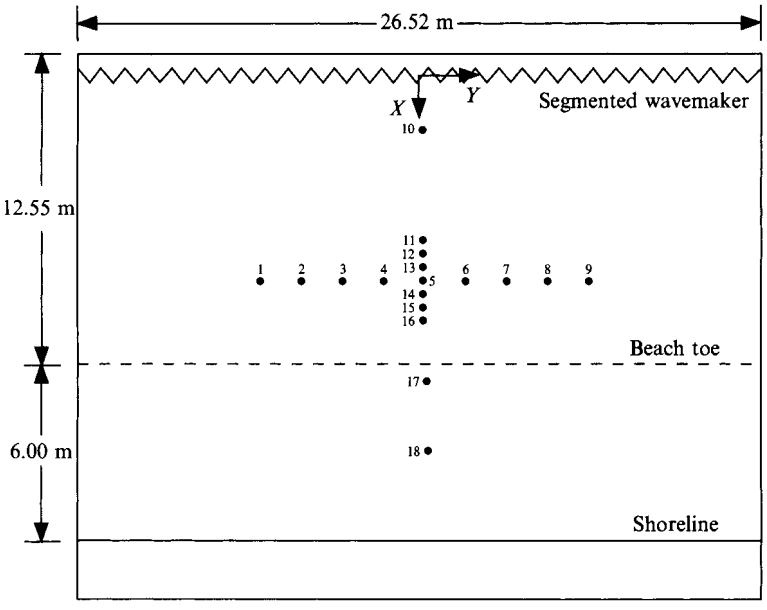

FIGURE 2. Schematic (planform) view of the wave basin, showing its segmented wavemaker (∿∿), uniform-depth section (h = 20 cm), and 1:30 sloping beach section. The locations of the wave gauges were as follows:

gauge	X(m)	Y(m)	gauge	X(m)	Y(m)	gauge	X(m)	Y(m)
1	8	−8	2	8	−6	3	8	−4
4	8	−2	5	8	0	6	8	2
7	8	4	8	8	6	9	8	8
10	2	0	11	6.5	0	12	7	0
13	7.5	0	14	8.5	0	15	9	0
16	9.5	0	17	13	0	18	16	0

paddles of the segmented wavemaker for each of the cnoidal wavetrains; the bb and BB are the wavelengths in m for each of the cnoidal wavetrains; and the cc and CC are crest amplitudes (i.e. maximum elevations above the mean water level) in cm for each of the cnoidal wavetrains. Ordinarily, the wavelengths and amplitudes of the two-dimensional wave patterns that resulted from these inputs differed slightly from these values. A 10 s-ramp was applied to the start of each command signal driving the wavemaker to protect the mechanical system from sudden starts. Hence, there is a 10 s transient period at each site in the basin before the programmed waves arrived.

Our primary means of wave measurement was a linear array of nine wave gauges that was parallel to, and 8 m from, the wavemaker astride the basin centreline (see figure 2). The nine capacitance-type gauges, spaced at 2 m intervals, measured the elevation of the water surface. A second array of similar gauges was placed normal to the wavemaker along the basin centreline. It contained eight gauges (one shared with the first array) in the uniform-depth section; seven spaced at 0.5 m intervals beginning 6.5 m from the wavemaker, and one 2 m from the wavemaker. (This array also contained two gauges in the sloping-beach section; data from these gauges are not reported here.) The wave gauges were calibrated and recording began in a quiescent basin immediately prior to starting the wavemaker. Continuous-time signals for 100 s were obtained from all 18 gauges; these signals were low-pass filtered using an 8-pole Butterworth filter with a 10 Hz cutoff, and then digitized to produce 25 Hz discrete-

time data. The algorithm to fit KP solutions to wave data, described in detail in Appendix B, is based solely on data from the nine-gauge array; i.e. we make no use of the wavemaker parameters, which are given in the experiment label. As stated earlier, the algorithm was designed in this way so that it could also be used for waves of unknown origin. Data from the second array are used in §4 to test predictions of the fitted solutions.

Wavefields were also measured qualitatively using two Hasselblad cameras, placed 6 m apart astride the basin centreline and 7 m above the nine-gauge array. The cameras took simultaneous overlapping pictures of the water surface in a darkened room using four 880 W-s strobe lights located on the beach and pointing toward the wavemaker. (The wave gauges were removed from the basin during photography.) The two photographs were then combined to form a mosaic, like those in figure 1. All photographs were printed so as to maintain the same horizontal scale, which is indicated by the (+) marks painted on the basin floor at 1 m intervals. The small, but measurable, differences in spacing between (+) marks apparent in figure 1 resulted from optical distortions by the waves, which acted like moving lenses. This distortion prevented us from using the overhead photographs to measure spatial wavelengths quantitatively.

Fifteen experiments on asymmetric waves were conducted in the set under discussion. In each experiment, a two-dimensional spatially periodic wave pattern was created at one end of the tank. The entire wave pattern propagated across the tank with nearly permanent form, it was recorded as it swept by the array of gauges, and then it was mostly absorbed on the sloping beach.

Figure 1 shows clear photographic evidence that two-dimensional approximately periodic waves exist in shallow water. Photographs of three different wave patterns, corresponding to three experiments are shown. Each wave pattern propagates from top to bottom in the photos; the front of each wave crest appears bright, while the back appears dark. Some of the bright–dark boundaries in figure 1 (*a*) are particularly sharp, indicating that these wave crests are particularly steep, and close to breaking. Close inspection of figure 1 (*a*) also shows that on the front faces of these steep waves are capillary waves that appear to be radiating from the crests, as expected for near-breaking waves. Thus, even though the KP equation is asymptotically valid only for waves of small amplitude, figure 1 (*a*) clearly demonstrates that two-dimensional, approximately periodic waves exist even at large amplitudes. The existence and stability of these waves seem to persist well beyond the putative range of validity of the KP model.

The wave pattern in figure 1 (*a*) is symmetric, like those discussed in Part 1, and the pattern propagates directly downward in the photograph, i.e. in the x-direction. The wave pattern in figure 1 (*b*) is slightly asymmetric, and that in figure 1 (*c*) is strongly asymmetric. Asymmetric waves propagate in directions oblique to the x-direction. A feature common to all of the waves in all of our experiments, including those in figure 1, is the basic hexagonal shape of the wave pattern. The basic template has a broad flat trough surrounded by six relatively narrow wave crests. One such hexagon is drawn in figure 1 (*b*). The wave crests opposite each other in this hexagon are parallel, they are equal in length and in wave amplitude, and they can be identified with each other in order to reproduce the periodic pattern, i.e. one can tile the plane with copies of this basic hexagon.

Figure 3 shows typical data obtained from the nine-gauge array for three experiments on asymmetric waves, including two that were photographed in figure 1 (*b*, *c*). (Note that the waves shown in figure 1 (*b*, *c*) represent about 3 s of data in figure 3 (*a*, *b*).) The

100 s records show an initially quiescent water level and the subsequent arrival of the generated wave pattern, whose first 10 s exhibit a transient caused by the ramped start of the wavemaker. Data taken during these intervals are excluded in subsequent analysis. (We note also that some wave reflection undoubtedly occurs on the 1:30 sloping beach, leading to small standing-wave components in the wave records. No attempt has been made to remove reflected waves from the data.) At first glance, data at each gauge site may appear to be periodic, especially in figure 3(*b*); however, careful examination shows that the periodicity is not exact, which is characteristic of quasi-periodic waves.

Figure 4 shows the amplitude–frequency spectrum of each of the wave records shown in figure 3(*b*). (The spectral amplitude is the modulus of the fast Fourier transform, or FFT, of the data. For convenience, we will refer to these amplitudes as FFTs.) To save space, we omit the spectra for the other experiments shown in figure 3, but these spectra are qualitatively similar to those shown here. Figure 4 shows clearly the characteristic signatures of two-dimensional nonlinear two-phase waves: each of the three FFTs shows two dominant frequencies, plus their harmonics and some sum and difference frequencies. As one moves from the FFT of one wave record to another within each experiment, the amount of energy (i.e. square of the spectral amplitude) at each frequency changes, but the total energy is always distributed among the same two frequencies, plus their harmonics. In this way, the FFTs for each experiment show that all of the gauges measured one-dimensional slices through the same two-dimensional wave pattern. The photographs in figure 1(*b*, *c*) show clearly the spatial pattern of two-dimensional two-phase waves, so one expects temporal FFTs like those in figure 4. However, based solely on the FFTs of wave-gauge data we could infer the following information directly.

(i) The wave pattern has two phases (or possibly more than two in degenerate cases, but with only two independent frequencies among the phases):

(ii) the wave pattern is nonlinear, because energies at harmonics as well as at the sum and difference frequencies are significant.

The fact that the same two frequencies are measured at every gauge, with different energy levels, suggests that the wave pattern might be two-dimensional, but it does not establish the two-dimensionality conclusively. If the wave pattern is genuinely two-dimensional with exactly two phases, then necessarily it is stationary in some uniformly translating coordinate system; i.e. it must be a wave of permanent form.

Figure 4 also lists the numerical values of the two fundamental frequencies measured in the experiment. The two-dimensional wave patterns shown in figure 1 are periodic, but the one-dimensional wave records in figure 3 are not periodic unless these two frequencies are rationally related. Since the frequencies listed in figure 4 were obtained numerically, they are necessarily rationally related. However, for experiment KP220203-110403, the period implied by the two frequencies exceeds 600 s, so this exact periodicity is irrelevant for the 100 s of recorded data, which are effectively quasi-periodic.

We note finally that quasi-periodic functions also arise in the theory of dynamical systems (e.g. Guckenheimer & Holmes 1983), where quasi-periodic behaviour often suggests incipient instability and chaos (Piexoto 1962). No such instability is suggested from the quasi-periodicity seen in figure 3. These data are quasi-periodic only because the data are taken from a doubly periodic function, along a line at an irrational angle from a direction of periodicity. The water waves being measured seem to be remarkably stable.

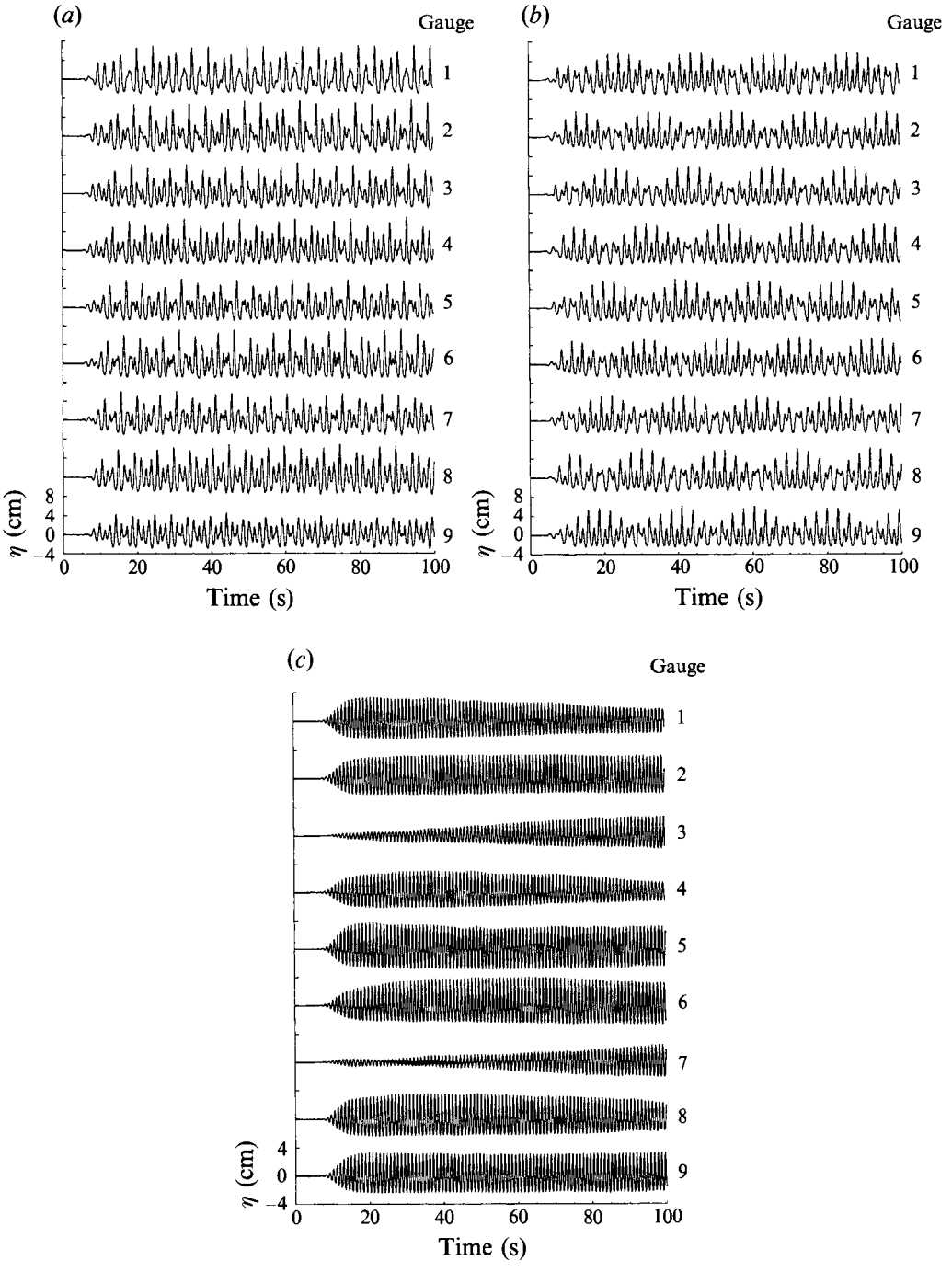

FIGURE 3. Data from the nine-gauge array, for three asymmetric wave patterns, including two shown in figures 1(*b*, *c*) Experiment: (*a*) KP400203-300303; (*b*) KP220203-110403; (*c*) KP300102-30·803.

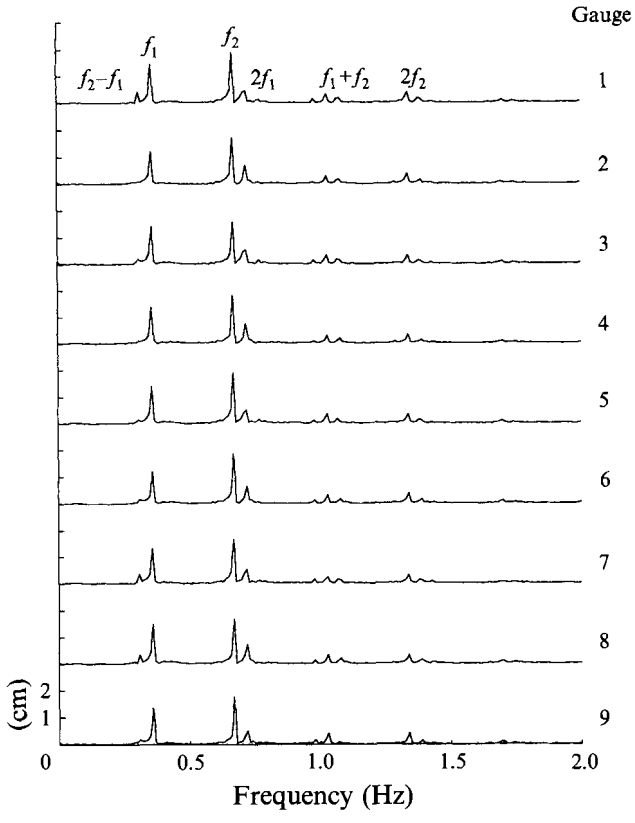

FIGURE 4. FFTs (periodograms) in T of the wave records shown in figure 3(b) for experiment KP220203-110403. Every FFT shows energy at the same two frequencies ($f_1 = 0.36$ Hz, $f_2 = 0.67$ Hz), plus their harmonics. The dominant harmonics have been identified in one FFT.

4. Comparison of theory and experiment

In Appendix B, we present an algorithm to find the KP solution of genus 2 that best fits experimental data like those shown in figure 3. Here is a brief summary of the algorithm. Recall from §2 that a KP solution of genus 2 is specified by eight real-valued parameters. Four of these (μ_1, μ_2, ν_1, ν_2) are wavenumbers that determine the overall spatial structure of the wave pattern. Two of them are easy to find: (μ_1, μ_2) are proportional to the two frequencies identified in figure 4. Once the spatial structure is known, then one varies (b, d, λ) in order to match (as closely as possible) the observed maximum and minimum amplitudes, and the known spatial structure. Then one determines the two phase constants (Φ_1, Φ_2) by minimizing the r.m.s. (or L_2) error for the entire wave pattern. Finally, with good approximations to the eight KP parameters determined in this way, one selects final values for all eight parameters by minimizing the r.m.s.-error for the wave pattern again. (Thus, the KP solution found in this way is 'best' in the sense of least r.m.s.-error.)

This algorithm was used to find the best KP solution for each of fifteen experiments with asymmetric wave patterns. We begin our discussion of results with the question: How accurately does the best KP solution represent the data used to select that solution? For conciseness, we concentrate on the three experiments shown in figure 3.

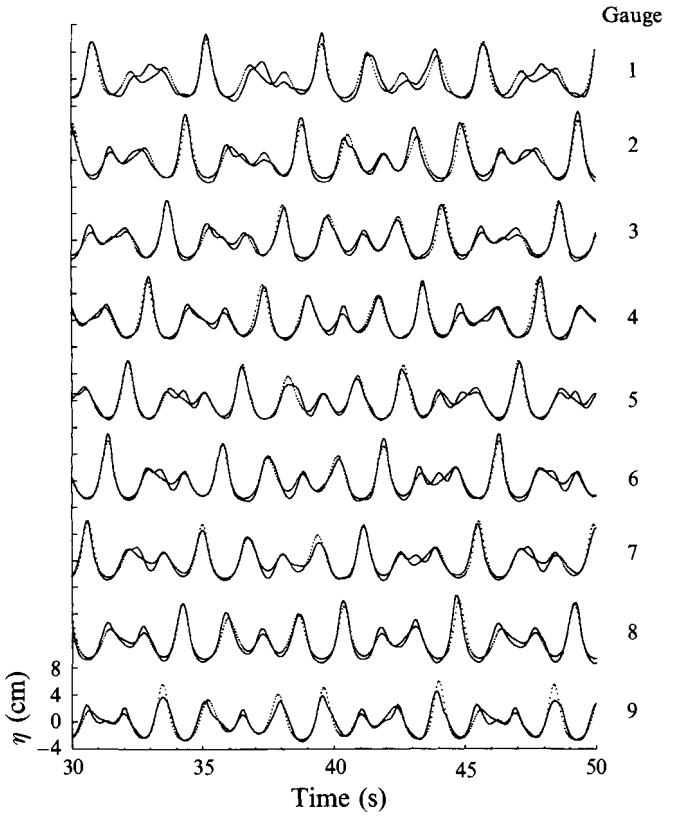

FIGURE 5. Detailed comparison of measured wave records (——) with the best KP solution (.....) at the same locations, for 20 s of data from experiment KP400203-300303. The comparison began 30 s into the experiment.

4.1. *Surface-fitting*

For the experiment shown in figures 1(*b*) and 3(*a*), figure 5 shows a comparison of the measured data to the best KP solution at the same locations, for 20 s of data, and for all of the gauges in the nine-gauge array. (Most of our comparisons begin 30 s into the recorded data in order to exclude the quiescent and transient intervals, and last for 20 s. The agreement between theory and experiment is largely independent of when we start the comparison and how long we compare.) The agreement between KP theory and experimental data in figure 5 is perfect nowhere, but it is fairly good everywhere. The KP solution captures the overall structure of the wave pattern; it describes the phase information, such as zero-crossings, particularly well. Note especially the amplitudes of the waves in figure 5. From figure 3, the maximum crest-to-trough height (H) for this wave pattern is 11.23 cm., which corresponds to a wave height-to-depth ratio (H/h) of 0.56. Peregrine (1983) discusses criteria for wavebreaking in shallow water (e.g. $H/h = 0.77$ at breaking). The wave pattern shown here is not breaking, but it is not far from the range of breaking waves; certainly the wave amplitudes are not especially small. This result is similar to that found in Part 1 for symmetric waves: KP theory agrees well with experimental measurements well outside its putative range of validity.

Figure 6 shows another comparison of theory and experiment, for the wave pattern

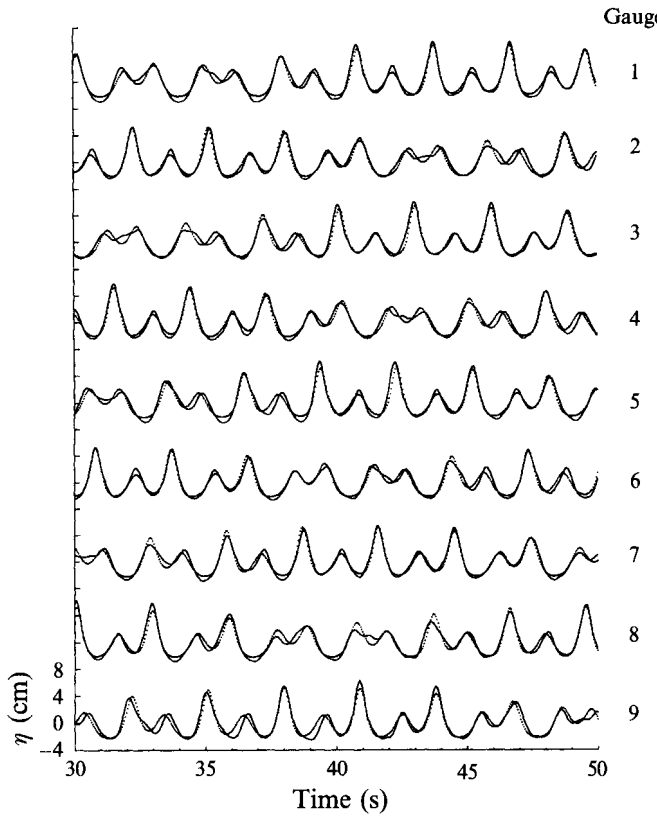

FIGURE 6. Detailed comparison of measured wave records (——) with the best KP solution (.....), for 20 s of data from experiment KP220203-110403, beginning at 30 s.

shown in figures 1(*c*) and 3(*b*). This pattern is strongly asymmetric, but again the best KP solution gives good agreement everywhere. Figure 3(*b*) shows that these waves are almost periodic, with an almost-period of about 20 s. Figure 6 shows that the KP solution has essentially the same behaviour. (In fact, the comparison time of 20 s was chosen to contain the almost-period of these waves.) Because this experiment was also photographed (in figure 1*c*), we can compare the KP solution with the photograph as well. In figure 7, contour lines of the best KP solution are superimposed on the photograph. This comparison contains different information than that in figure 6: X is held fixed while T and Y vary in figure 6, whereas T is held fixed while X and Y vary in figure 7. Moreover, the photograph was not used to find the KP solution, so figure 7 is *not* surface-fitting. Even so, figure 7 leads to a conclusion similar to that obtained from figures 5 and 6: the best KP solution describes the observed wave pattern with reasonable accuracy everywhere.

The last detailed comparison, for KP300102-30·803, has been included because the wave records from gauges 3 and 7 showed a slow increase in amplitude over the course of this experiment, as seen in figure 3(*c*). While it is clear that the data in figure 3(*b*) are almost periodic, this is much less clear in figure 3(*c*), so this experiment provides a strong test of the theory. Figure 8(*a*) shows a comparison of the measured wave records with the best KP solution, for 20 s of data starting at 30 s. These waves have smaller amplitudes than those in other experiments in this series, so the waves are more

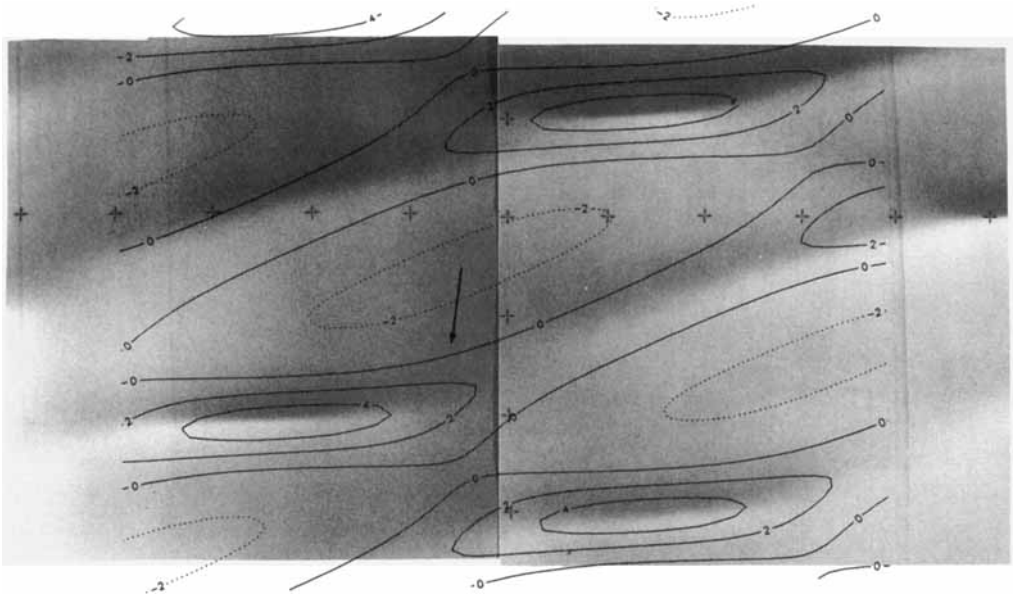

FIGURE 7. For experiment KP220203-110403, contour lines of the best KP solution (identified in figure 6) are superimposed on the photograph of figure 1(*c*). The experiment and the KP solution are the same as in figure 6, but different data are compared. The direction of propagation of the entire wave pattern, based on (8) is shown by the arrow.

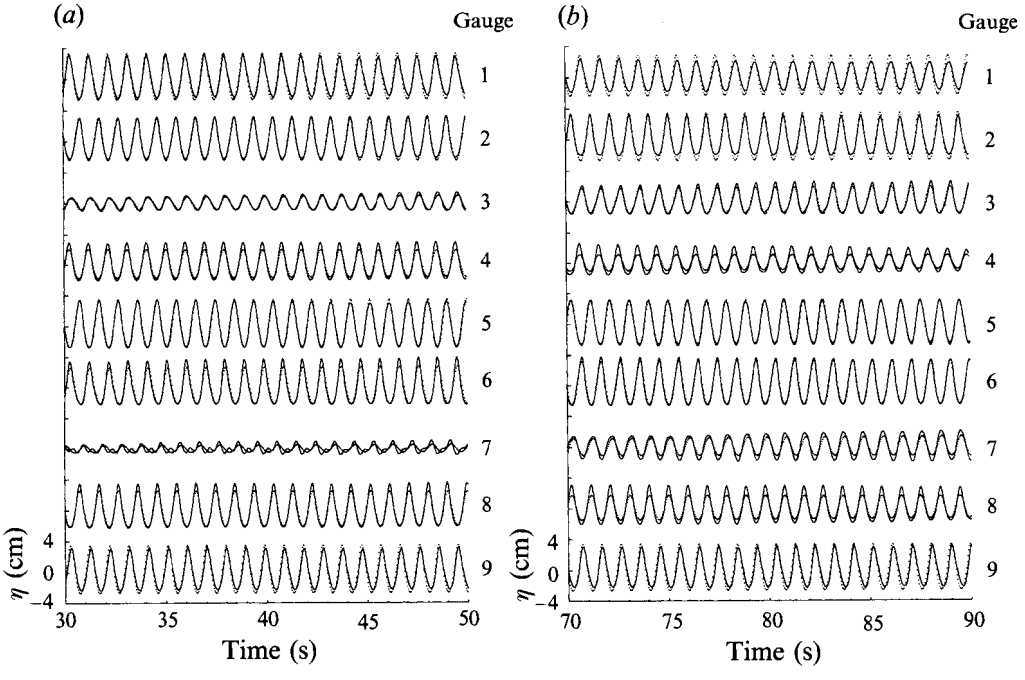

FIGURE 8. For experiment KP300102-30·803, a detailed comparison of measured wave records (——) with the best KP solution (……), during two different time intervals: (*a*) 20 s of data beginning at 30 s; (*b*) 20 s of data beginning at 70 s.

	KP Parameters											Errors	
Case	$-b$	λ	$-d$	μ_1	μ_2	ν_1	ν_2	ω_1	ω_2	η_{max}	η_{min}	f_{max}/u_{max}	σ
000203-380203	4.56	0.403	3.95	0.602	0.600	0.004	−0.296	0.091	−0.355	5.81	−3.46	0.851	0.297
100203-150203	4.58	0.540	3.28	0.602	0.602	−0.155	0.073	0.029	0.069	5.66	−3.38	0.921	0.369
050203-050303	3.20	0.723	2.86	0.419	0.602	−0.038	0.037	−0.033	0.114	7.35	−3.24	0.666	0.402
150203-050303	3.42	0.580	3.23	0.421	0.601	−0.038	0.116	−0.052	0.029	6.84	−3.26	0.721	0.348
250203-100303	3.44	0.423	3.74	0.421	0.601	−0.076	0.191	−0.109	−0.110	7.50	−2.76	0.791	0.312
100203-250303	3.32	0.393	3.95	0.421	0.601	−0.191	0.076	−0.328	0.036	7.48	−2.56	0.815	0.305
200203-200303	3.39	0.365	3.98	0.421	0.601	−0.154	0.150	−0.237	−0.044	8.25	−2.74	0.723	0.312
300203-200303	3.44	0.295	4.11	0.420	0.601	−0.154	0.229	−0.235	−0.186	7.71	−2.90	0.789	0.267
220203-110403	2.89	0.382	4.12	0.322	0.601	−0.085	0.168	−0.140	−0.035	6.29	−3.11	0.843	0.282
350203-150303	3.49	0.302	4.14	0.421	0.601	−0.116	0.269	−0.155	−0.278	7.94	−2.83	0.755	0.283
400203-300303	3.47	0.196	4.27	0.421	0.601	−0.224	0.305	−0.409	−0.376	7.60	−3.62	0.819	0.312
300203-300102	4.46	0.377	6.29	0.601	0.933	0.232	−0.225	−0.137	0.551	5.80	−3.47	0.769	0.235
300203-30·803	4.46	0.376	6.05	0.601	0.936	0.299	−0.232	−0.135	0.545	6.42	−3.77	0.720	0.311
250203-450102	4.49	0.353	6.47	0.600	0.933	0.189	−0.342	−0.045	0.342	5.48	−3.49	0.777	0.252
300102-30·803	6.50	0.412	5.97	0.933	0.932	−0.234	0.227	0.577	0.575	3.96	−2.88	0.890	0.248

TABLE 1. Summary of comparisons between KP theory and experiments

nearly sinusoidal, and the agreement between theory and experiment is slightly better than average. Note that the wave amplitudes for gauges 3 and 7 increase, even in this 20 s interval. Note also that for gauge 3, the KP solution captures this behaviour.

Figure 8(*b*) shows a second comparison for the same experiment, KP300102-30·803, starting at 70 s. It is important to note that the KP solution used here is the same KP solution as that in figure 8(*a*), except that the two phase variables, Φ_1 and Φ_2, were reoptimized for the new data, which were measured during a different time interval. In other words, figure 8(*b*) is not a surface-fit; it is a prediction of the theory, based on the surface-fit shown in figure 8(*a*). Figure 3(*c*) shows that the data measured at 20 s differ considerably from those measured at 70 s, but the same KP solution describes both data sets with reasonable accuracy. This good agreement implies that the data in figure 3(*c*) are almost periodic, but the almost-period is so much longer than the 80 s of data that this feature is not apparent in the measured data. We mention that we also applied the optimization algorithm to the data in figure 8(*b*), to find the best KP solution for those data. The KP solution found was nearly identical with that obtained from the data in figure 8(*a*), except for changes in Φ_1 and Φ_2.

4.2. *Analysis of errors*

Table 1 summarizes the comparisons between KP theory and experiments for fifteen experiments involving asymmetric waves. The parameters of the best KP solutions are listed, as well as the maximum and minimum measured wave amplitudes, and two measures of error, which we now define.

For a given experiment, let $u(x, y, t)$ denote the measured wave amplitude at location (x, y, t), normalized as in (2), and let $f(x, y, t)$ denote the value of the best KP solution at the same location. One measure of their discrepancy is σ, where

$$\sigma^2 = \sum_1^9 \int_0^L [f(x,y,t) - u(x,y,t)]^2 \, dx \Big/ \sum_1^9 \int_0^L [u(x,y,t)]^2 \, dx, \tag{10}$$

the sum is taken over the wave records from the nine-gauge array, and L is the length of the measured wave records. (We generally used 20 s of data, but varying the length of the data string did not significantly affect σ.) A second measure of error is f_{max}/u_{max}, the ratio of maximum wave amplitudes according to theory and experiment. (Step 4 of the optimization algorithm effectively minimizes $(1 - f_{max}/u_{max})^2$, but then the last step of the algorithm usually forces it away from its minimal value, leaving f_{max}/u_{max} as a non-trivial measure of error.)

According to table 1, the KP model along with the optimization algorithm consistently underpredicted the maximum wave amplitude. This error was more serious in some experiments than in others, but the model predicted a maximum amplitude that was too small in every experiment. This consistent underprediction was apparently caused by using the norm in (10). In Part 1 we used a different norm, and matched the maximum amplitudes well. Beyond this simple observation, we found no striking trends in the data. For all fifteen experiments, σ stayed within a fairly narrow range: $0.235 \leqslant \sigma \leqslant 0.402$, with a mean value of $E(\sigma) = 0.302$. (For comparison, note that the trivial theory, in which $f(x, y, t) \equiv 0$, gives $\sigma = 1$ in (10).) We do not suggest from this relatively narrow range of values that the theory never breaks down, but only that our experiments did not demonstrate the breakdown.

As mentioned in §2, the KP model of water waves is based on three assumptions: (i) moderate wave amplitudes; (ii) shallow water; and (iii) nearly one-dimensional wave propagation. An important question is how σ depends on each of these three effects. Consider first the wave amplitudes, which we characterize by the maximum

crest-to-trough height, divided by the undisturbed water depth, which was 20 cm in these experiments. (This choice is based on the columns entitled η_{max} and η_{min} in table 1, and is somewhat arbitrary. We also tried using η_{max}, with similar results. Using σ, instead of σ^2 or some other measure of error, is also arbitrary.) For the jth experiment, let

$$A_j := [\eta_{max,j} - \eta_{min,j}]/h. \tag{11}$$

From table 1, $0.341 \leqslant A_j \leqslant 0.561$, with a mean value, $E(A) = 0.492$. The correlation coefficient between A and σ in our fifteen experiments is

$$\rho(A,\sigma) := \frac{\sum^{15} [A_j - E(A)]^* [\sigma_j - E(\sigma)]}{\{\sum^{15} [A_j - E(A)]^2 * \sum^{15} [\sigma_j - E(\sigma)]^2\}^{1/2}} = 0.39. \tag{12}$$

This positive correlation shows that KP theory becomes less accurate as wave amplitudes increase, as expected.

It remains to test the assumptions of shallow water, and of nearly one-dimensional waves. Unfortunately, our data set (based on fifteen experiments) was too small to carry out these tests conclusively.

4.3. *Predictions*

Knowing that the KP model provides reasonably accurate descriptions of the measured wavefields, we now turn to other comparisons between theory and experiments. For each experiment, the best KP solution is now fixed, with no remaining free parameters; hence, the comparisons that follow involve predictions of the theory, rather than just surface-fitting.

A fundamental assertion in this paper is that the waves under study propagate with nearly permanent form. Yet data from the nine-gauge array cannot test this assertion, because all nine gauges are the same distance from the wavemaker. Limited insight into possible wave evolution is provided by the second gauge array, which was placed perpendicular to the first array (see figure 2). We show next that, to within our experimental error, the waves did not evolve significantly over the 7.5 m span of the second array. Again, for simplicity, we concentrate on the three experiments shown in figure 3.

For each experiment, the second gauge array provides eight wave records like those in figure 3. Figure 9 shows the temporal FFT of each of the seven new wave records for experiment KP220203-110403, featured in figures 1(*c*), 3(*b*), and 4. (Note from figure 2 that gauge 5 was included in both arrays. In presenting the data from the second array, we omit gauge 5 because its data were already presented. We also omit the data from the other experiments, which data were qualitatively similar to those shown in figure 9.) Note that every gauge in the second array recorded the same two dominant frequencies, and therefore the same values for μ_1 and μ_2; in other words, μ_1 and μ_2 showed no measurable evolution as the waves propagated away from the wavemaker.

Figure 10 shows the actual wave records from the seven new gauges, for experiment KP220203-110403. The KP solution that was already selected, based on data from the nine-gauge array, predicts the data that each of these seven gauges should measure; these predictions are also shown in figure 10. We emphasize that no free parameters were available in the comparisons in figure 10; these are predictions rather than surface-fits. The overall error (σ_χ) for the seven-gauge array is comparable to that for the nine-gauge array (σ), even though data from the latter array were used to select the KP

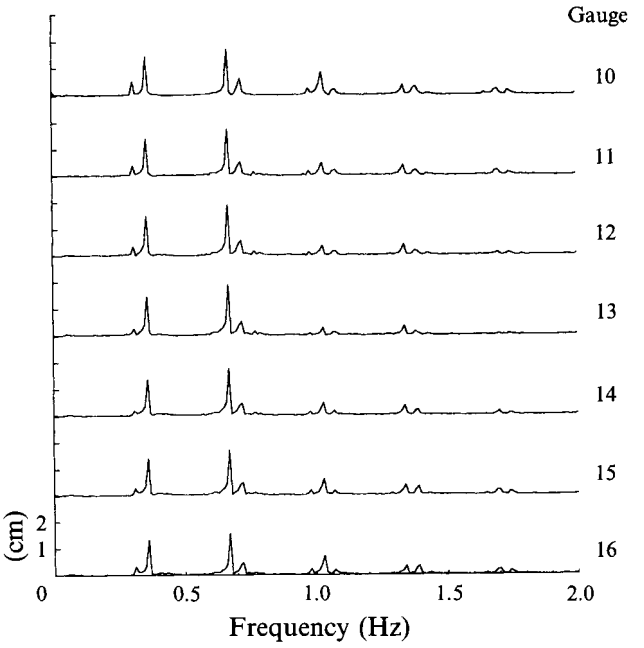

FIGURE 9. Temporal FFTs of the seven wave records obtained from the second gauge array, for experiment KP220203-110403.

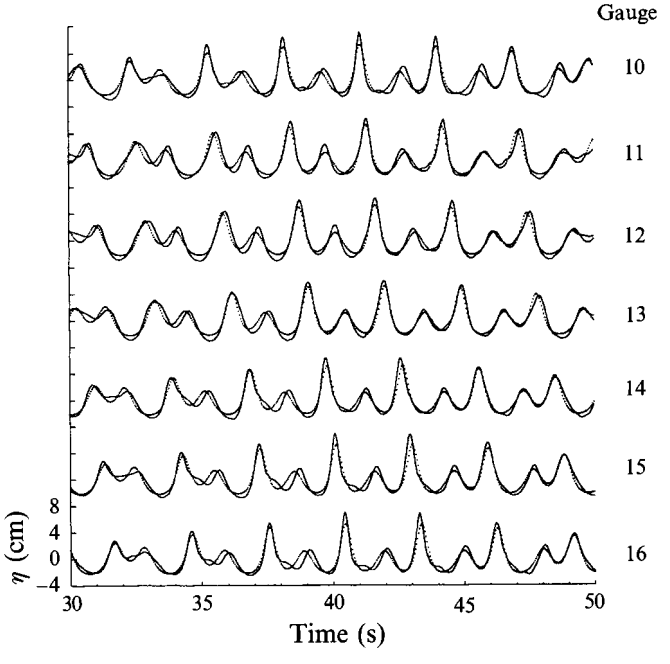

FIGURE 10. Superposition of the measured wave records from the seven-gauge array (——), and the wave pattern predicted by the KP solution chosen to fit the data from the nine-gauge array (.....), for experiment KP220203-110403.

	Theoretical		Experimental			
Case	dx/dt	dy/dt	dx/dt	dy/dt	σ	σ_χ
000203-380203	−0.141	−1.484	−0.164	−1.503	0.297	0.326
100203-150203	−0.087	−0.202	−0.115	−0.171	0.369	0.403
050203-050303	−0.083	−1.771	−0.084	−1.953	0.402	0.422
150203-050303	0.067	−0.607	0.060	−0.609	0.348	0.358
250203-100303	0.231	−0.154	0.219	−0.167	0.312	0.350
100203-250303	0.123	−1.452	0.112	−1.460	0.305	0.307
200203-200303	0.271	−0.799	0.249	−0.805	0.312	0.316
300203-200303	0.436	−0.335	0.419	−0.338	0.267	0.314
220203-110403	0.251	−0.688	0.243	−0.685	0.281	0.319
350203-150303	0.403	0.133	0.387	0.126	0.283	0.299
400203-300303	0.800	−0.340	0.786	−0.333	0.308	0.282
300203-300102	−0.286	1.302	−0.291	1.308	0.235	0.287
300203-30·803	−0.264	1.283	−0.277	1.293	0.311	0.316
250203-450102	−0.129	0.646	−0.144	0.663	0.252	0.305
300102-30·803	−0.618	0.008	−0.612	0.006	0.248	0.294

TABLE 2. Comparison between theory and experiment of two components of the velocity of propagation of the wave pattern, and the overall error from the nine-gauge array (σ) and the seven-gauge array (σ_χ)

solution. For all fifteen experiments on asymmetric waves, table 2 lists an overall error (σ) for the nine-gauge array used to select the KP solution, and another (σ_χ) for the seven-gauge array, whose measurements were predicted by that KP solution. Within each experiment, these errors are comparable; usually σ_χ is slightly larger than σ, but for experiment KP400203-300303, the error for the seven-gauge array (σ_χ) is actually smaller than that for the nine-gauge array (σ). This comparison supports the claim that the measured waves did not evolve significantly over the length of our test section.

Approximate wavelengths in the X-direction for a KP solution can be obtained from $\{\mu_1, \mu_2\}$, using $L_i \approx 2\pi h/\mu_i$. For experiment KP220203-110403, this gives X-wavelengths of about 2 m and 4 m, consistent with the cnoidal wavelengths input to the wavemaker. Note that gauge 10 is only 2 m from the wavemaker, so figure 10 shows that the wave being measured achieved its apparently permanent form within one wavelength of the wavemaker, and then retained that form at least for the length of the test section of the tank (7.5 m). In all fifteen experiments, we always found that the wave patterns achieved their apparently permanent form within 2 m of the wavemaker, and then retained that form over the length of our test section. We found no clear evidence of wave evolution.

Next, we consider the (constant) velocity of propagation of the waves. This velocity cannot be inferred from the photographs in figure 1. The KP model predicts it, in (8), and the velocity vector shown in figure 7 was found in this way. However, the velocity also can be obtained directly from the wave records, without using (8), as follows. For a particular experiment, find the KP solution that best fits the data measured during a 20 s interval starting at time (T). If the wave has permanent form, then at a slightly later time ($T+\Delta T$), this wave pattern will have translated in space, and what had been observed at location ($X-\Delta X$, $Y-\Delta Y$) in the fixed (laboratory) frame now will be observed at (X, Y), for some $\{\Delta X, \Delta Y\}$. In order to measure $\{\Delta X, \Delta Y\}$, use (2) to replace (6) by

$$\phi_j = \mu_j(x-\Delta X/h)+\nu_j(y-\Delta Y/h)+\omega_j(t-\Delta X/6h)+\Phi_j \quad (j=1,2) \tag{13}$$

and then minimize σ^2 at the new time (i.e. over 20 s starting at $T+\Delta T$) by varying $\{\Delta X, \Delta Y\}$, holding fixed all the other parameters of the solution. In this way, one obtains empirically $\{\Delta X, \Delta Y\}$ for a given ΔT. For a wave of permanent form, $(\Delta X/\Delta T)$ and $(\Delta Y/\Delta T)$ do not depend on ΔT, and it follows from (2) that

$$\frac{\mathrm{d}x}{\mathrm{d}t} = 6\left(1-(gh)^{1/2}\frac{\Delta T}{\Delta X}\right), \quad \frac{\mathrm{d}y}{\mathrm{d}t} = 6\frac{\Delta Y}{\Delta X}. \tag{14}$$

Because the KP solution is spatially periodic, $\{\Delta X, \Delta Y\}$ are ambiguous in the sense that one can add to them an integer number of spatial periods of the wave pattern. One eliminates this discrete ambiguity by requiring that $\Delta X \to 0$, $\Delta Y \to 0$ as $\Delta T \to 0$; then $\{\Delta X, \Delta Y\}$ are unambiguous for ΔT small enough. On the other hand, small measurement errors become relatively important if ΔT is too small. Balancing these competing effects, we chose $\Delta T = 1.2$ s for these experiments.

Table 2 lists the two components of the velocity of propagation of the wave pattern, according to KP theory (8) and according to direct measurement (14), for all fifteen experiments. The agreement is remarkably good; in many cases, the two velocities agree to within a few percent. The agreement becomes even more impressive when one recalls that these velocities are themselves the small deviations from the basic wave speed, $(gh)^{1/2}$, which is inherent in the (moving) KP coordinate system.

5. Oceanic observations of hexagonal waves in shallow water

The central point of this paper is the following. In shallow water of uniform depth, there exist two-dimensional periodic waves with finite amplitudes and nearly permanent form. The spatial pattern of these waves is hexagonal, as shown in figure 1. The waves are easy to generate in the laboratory, and they are apparently stable.

KP solutions of genus 2 describe these waves with reasonable accuracy over a range of parameters that is larger than the putative range of validity of the KP model. The robustness of the KP model is a pleasant surprise, but we suspect that the existence of these waves is independent of the validity of the KP model. Rather, we conjecture that the hexagonal wave pattern observed in figure 1 is the basic qualitative pattern for periodic waves of permanent form in shallow water. More precisely, we conjecture that if one seeks genuinely two-dimensional wave patterns of finite amplitude that are periodic and that propagate with permanent form in shallow water of uniform depth, then one will almost certainly find hexagonal wave patterns with flat troughs and narrow crests, like those in figure 1. If this conjecture is correct, then one would expect to find waves like these in oceanic settings. In this section, we present some oceanic observations suggesting that wave patterns like these actually occur.

Remark: Some apparent counter-examples to this conjecture are actually limiting cases of it. We mention specifically: (i) cnoidal waves, in which the wave period in one direction becomes infinitely long; (ii) waves of infinitesimal amplitude, for which the hexagon degenerates to a parallelogram, and the waves become sinusoidal; and (iii) the oblique interaction of two solutions, which is not periodic, but is another limiting case of hexagonal waves.

The first example, shown in figure 11, is an aerial photograph of the coastal zone taken near Jones Inlet on Long Island near New York City. At the top of the photograph one can identify a road, some buildings, the beach, and the surf zone in which waves are breaking. Beyond the surf zone, in the bottom half of the photograph, one sees clearly that the surface wave patterns are two-dimensional and approximately periodic, like the waves in figure 1, and that many of the wave patterns are hexagonal.

FIGURE 11. Aerial photograph of waves off the southern coast of Long Island. The beach is between Lido Beach and Point Lookout, west of Jones Inlet. Beyond the surf zone, the wave patterns are two-dimensional, and approximately periodic. They have flat troughs, sharp crests, and approximately hexagonal shape.

The second example, shown in figure 12, is a now well-known photograph taken by Terry Toedtemeier of two waves interacting in shallow water off the Oregon coast. This photograph is often shown to illustrate the interaction of two solitons, with the required phase shift (i.e. a spatial shift of each wave crest as a result of the nonlinear interaction of the two waves). However, each of the most prominent wave crests in figure 12 is actually part of a train of periodic waves. The next crest in each train is discernible in the figure, but the strongest evidence of the periodicity of the wavefield is that Mr Toedtemeier told us that the waves were periodic. He also noted that none of the other wave interactions, before or after the one shown in figure 12, was nearly as dramatic as the one shown. Thus, these waves were only approximately periodic, but they were certainly two-dimensional, and they exhibited flat troughs and sharp crests. In our model, the two long crests and the one short crest shown in the figure should be viewed as the sides of two adjacent hexagons.

The last example, shown in figure 13, is an aerial photograph of waves off the outer banks of North Carolina taken by Carl Miller during a major storm (the 'Hallowe'en storm of 1991'). The waves in this photograph were enormous – wave gauges located in 10 m deep water measured waves with heights exceeding 5 m and periods of 20 s. If we take the wave speed to be $(gh)^{1/2}$ as a rough approximation, then a wave period of 20 s corresponds to a wavelength of about 200 m. (Assigning a width of 5 m to the road visible along the coast and then scaling also suggests wavelengths on the order of 100–200 m). The photograph itself suggests that virtually every wave crest was breaking, and that the beach on the right of the photo was completely flooded. These waves were apparently far outside the range of validity of the KP model. Moreover, these waves undoubtedly did not have permanent form, so that KP solutions of genus

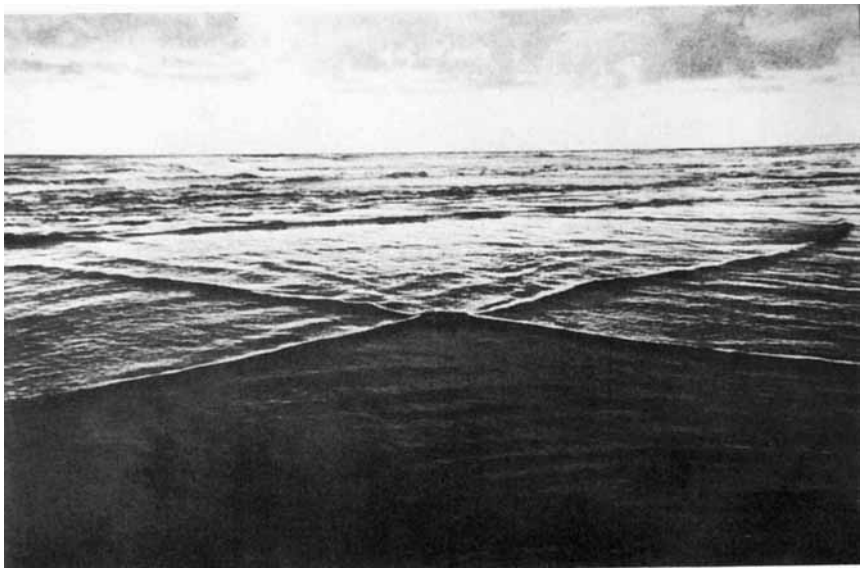

FIGURE 12. Oblique nonlinear interaction of two waves in shallow water, off the coast of Oregon. The interaction occurred in water about 1 m deep. (Photograph courtesy of T. Toedtemeier.)

FIGURE 13. Aerial photograph of waves in shallow water, south of the Oregon Inlet on Pea Island, off the coast of North Carolina. (Photograph courtesy of C. Miller.)

2 would be too simple to describe them. Nevertheless, the waves in figure 13 exhibit some of the same features that we have now seen repeatedly: two-dimensional wave patterns with flat troughs and sharp crests, and with many of the crests forming hexagonal wave patterns.

The photographs in figures 11, 12 and 13 suggests that approximately periodic, hexagonal wave patterns occur in the ocean. Without a systematic study of oceanic observations of waves in shallow water, we do not know whether these waves are

common or uncommon. We suspect that they are more common than is usually believed.

We are grateful to Boris Dubrovin and James Curry for useful comments and encouragement, and we thank Terry Toedtemeier and Carl Miller for permission to use the photographs in figures 12 and 13, respectively. Laura Mather and David Deininger provided useful programming assistance. We gratefully acknowledge the support and cooperation of the Coastal Engineering Research Center, US Army Engineer Waterways Experiment Station in Vicksburg, MS, which made these experiments possible, and we thank the Office, Chief of Engineers, US Army Corps of Engineers for authorizing publication of this research. This work was supported in part by ONR grant N00014-92-J-1274. Finally, we were saddened to learn that V. I. Petviashvili passed away in July 1993.

Appendix A. To obtain the program DELTA

The KP solutions used in this paper were computed using a FORTRAN program named DELTA. The following instructions show how to use the UNIX `ftp` utility to transfer the file `'delta.f'` from the anonymous site `'ftp.colorado.edu:/cuboulder/appm'`. The indented lines are keyboard commands, with `<cr>` = carriage return.

To log onto the `ftp` site, type

    ftp ftp.colorado.edu<cr>

You should get a prompt for a username. Type

    anonymous<cr>

You will then be prompted for a password. Enter your complete email address. At this point, you should be logged onto the `ftp` site.

You need to go to the subdirectory `/cuboulder/appm`. Type

    cd cuboulder/appm<cr>

To transfer the file, type

    get delta.f<cr>

To quit the `ftp` utility, type

    quit<cr>

Appendix B. An algorithm to find the best KP solution for a set of wave-gauge data

A KP solution of genus 2 is defined by (6+2) parameters $\{b, \lambda, d, \mu_1, \mu_2, \nu_2; \Phi_1, \Phi_2\}$, from which the other parameters of the solution $\{\nu_1, \omega_1, \omega_2\}$ can be deduced. The objective of this Appendix is to provide an effective algorithm to identify a 'best' set of KP parameters for a given set of wave records, like those in figure 3. The algorithm has six steps, and it makes explicit use of the fact that the time-variation of a quasi-periodic function, like that of (5) and (6), corresponds to straight-line motion on a two-dimensional torus.

Step 1: *Find* μ_1 *and* μ_2

If the measured wave amplitudes can be represented by a KP solution of genus 2, then it follows from §2 that we seek a function of the form

$$f(x, y, t) = F(\mu_1 x + \nu_1 y + \omega_1 t,\ \mu_2 x + \nu_2 y + \omega_2 t),$$

where F is periodic in each argument. Without loss of generality, we can require that each period be 2π; otherwise, the precise form of F does not affect step 1. In terms of laboratory coordinates, after using (2) with $\epsilon = 1$,

$$f = F(\mu_1[X-(gh)^{1/2}T]/h+\nu_1 Y/h+\omega_1 X/6h,\ \mu_2[X-(gh)^{1/2}T]/h+\nu_2 Y/h+\omega_2 X/6h). \tag{B 1}$$

Each wave gauge records data as T varies, with X and Y fixed. If it records a function in the form (B 1), then the FFT of the wave record shows energy at two frequencies, $(gh)^{1/2}\mu_1$ and $(gh)^{1/2}\mu_2$, plus harmonics and sum- and difference-frequencies. In other words, one can read $|\mu_1|$ and $|\mu_2|$ directly from FFTs of the wave records, like those in figure 4. Because of (7), one can always require $\mu_1/\mu_2 \geqslant 0$. Because Θ is even $[\Theta(\phi_1, \phi_2) = \Theta(-\phi_1, -\phi_2)]$, one can always take $\mu_1 \geqslant 0$, $\mu_2 \geqslant 0$. These two symmetries allow us to determine μ_1 and μ_2 from FFTs.

Remark. The advantage of the choice of variables in (2) is that it permits direct measurements of μ_1 and μ_2. With the usual choice, $t = \epsilon^{3/2}(gh)^{1/2}T/6h$, the FFTs yield $(\mu_1-\omega_1/6)$ and $(\mu_2-\omega_2/6)$ and one must solve to find μ_1 and μ_2. We have tried both approaches; the final results differ only slightly, and the logic of the current approach is simpler.

Step 2: *Find* $|\nu_1|$ *and* $|\nu_2|$

In these experiments we used only nine gauges at different locations in Y, so a Fourier transform in Y of the data at fixed (X, T) would yield only crude estimates of $|\nu_1|$ and $|\nu_2|$. We obtain more precise estimates of $|\nu_1|$ and $|\nu_2|$ when the wave height is a quasi-periodic function of two variables, as follows.

Let $F(\phi_1, \phi_2)$ be continuous and quasi-periodic. Along the line $[\phi_1 = \alpha\phi_2+\beta]$ in the (ϕ_1, ϕ_2)-plane, $F(\phi_1, \phi_2)$ is periodic if and only if α is rational. If α is irrational, then along this line $F(\phi_1, \phi_2)$ never repeats exactly, but it comes arbitrarily close to every value taken by $F(\phi_1, \phi_2)$ in the periodic square. Now compare this situation to that in figures 1 and 3. Figure 1 shows a periodic function of two variables, and each wave record shown in figure 3 is taken along a straight line defined by the direction of travel of the wave pattern as it sweeps past the gauges. It follows that if the data in each record are not periodic, then a sufficiently long string of data from a single gauge would eventually record the entire two-dimensional wave pattern, to any desired accuracy. Moreover, the nine gauges sweep out nine parallel line-segments in the (ϕ_1, ϕ_2)-plane. If the data are not periodic, then to any desired accuracy, one can think of these nine line-segments as segments on the same (infinite) line, with different starting points.

For example, in figure 3(*b*), the data recorded on gauge 9 nearly coincide with those recorded on gauge 3, but with a time-shift of 36.8 s. This can be seen directly, by laying a record from gauge 9 over that from gauge 3 (but shifted by 36.8 s) and observing that the data nearly coincide. More quantitatively, the two data sets (with the first 20 s of each data-set deleted, to remove quiescent and transient intervals) have a correlation coefficient of $\rho = 0.966$, where

$$\rho = \int_0^L \eta_i(t)\,\eta_j(t)\,\mathrm{d}t \Big/ \left[\int_0^L \eta_i(t)^2\,\mathrm{d}t \int_0^L \eta_j(t)^2\,\mathrm{d}t\right]^{1/2}, \tag{B 2}$$

and where $\eta_i(t)$ and $\eta_j(t)$ each have zero mean. Moreover, using the same time-shift (36.8 s), the data from gauge 8 correlate with those from gauge 2 (with $\rho = 0.966$), and gauge 7 reproduces the data from gauge 1 (with $\rho = 0.975$). In other words, with an error corresponding to a correlation coefficient of about 0.97, a shift in Y of 12 m (the distance between correlated gauges) is equivalent to a shift in T of 36.8 s. We have just

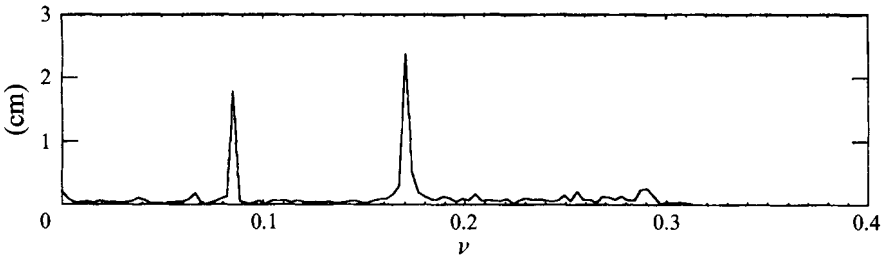

FIGURE 14. FFT in Y of the wave records for experiment KP220203-110403, after extension as described in the text.

demonstrated this with three pairs of gauges: $9 \rightarrow 3$, $8 \rightarrow 2$, $7 \rightarrow 1$. By this reasoning, had there been a 'virtual' gauge 10 in the shore-parallel array, it would have measured a signal (nearly) equal to that measured by gauge 4, but shifted by 36.8 s. Moreover, virtual gauge 11 would have measured a signal corresponding to that of gauge 5, and so on. Eventually, when we return to gauge 9 (at virtual gauge 15), we could start again by comparing its signal to that of gauge 3 again. This entire process can be repeated until we have shifted (in time) to the end of the data records. In addition, the data from a single gauge can be matched to itself in a second, independent way, and between these two shifts we can extend the data indefinitely. Referring again to figure 3(*b*), note that the data from any one gauge are almost periodic, with an almost-period of 41.84 s. In particular, in figure 3(*b*) the correlation coefficient between the data, and the data shifted by 41.84 s averages about 0.99 for gauges 4–9. By making use of these two kinds of shifts, one can create as many virtual gauges as desired. Each shift introduces a small error, whose size is related to $(1-\rho)$. In principle, one should stop adding virtual gauges when the accumulation of these errors exceeds the increased precision obtained from adding more gauges. Preliminary tests suggested that the break-even point for these data occurs at about 200 gauges; in practice, we always stopped at 200 gauges, including the 9 original gauges.

Now take a FFT in Y at fixed (X, T), based on 200 data points; the results are shown in figure 14, for experiment KP220203-110403. As in figure 4, the energy is concentrated in two dominant 'frequencies', plus harmonics and sum- and difference-frequencies. Assuming that the data represent a function of the form (10), then these dominant frequencies are located at $|\nu_1/h|$ and $|\nu_2/h|$. In this way, the procedure provides direct measurement of $|\nu_1|$ and $|\nu_2|$. This procedure does not specify which of the two values should be associated with μ_1, and which with μ_2. Until this has been resolved (in step 3), let us call the two values $|\nu_a|$ and $|\nu_b|$, with $|\nu_a| \leqslant |\nu_b|$.

Step 2a: Symmetric waves

The essential requirements for step 2 are that the data be quasi-periodic, but not strictly periodic. If the data are periodic with a sufficiently short period, then the wave records from two different gauges might never look alike, for any time-shift. In particular, symmetric waves produce periodic wave records, and the records from different gauges look alike only if two of the gauges happen to be an integer number of Y-wavelengths apart. For symmetric (or nearly symmetric) waves, we estimate the Y-wavelength from a FFT based on only nine gauges. This estimate is necessarily crude. Consequently, for some experiments with symmetric waves, we found it necessary to admit two or three 'candidate values' for $|\nu_a|$ ($= |\nu_b|$ for a symmetric wave), chosen from the range allowed by the nine-gauge FFT.

The remaining steps of the algorithm assume that the wave pattern is asymmetric, that the data are not strictly periodic, and that step 2 has successfully provided $|\nu_a|$ and $|\nu_b|$. (For symmetric waves, $\mu_2 = \mu_1$, $\nu_2 = -\nu_1$, so step 3 is unnecessary. Then step 4 simplifies, because $d = b(1-\lambda^2)$.)

Step 3: *Identify* ν_1 *and* ν_2

The next step is to find the signs of ν_a and ν_b, and to determine which value goes with μ_1, and which with μ_2. The basic idea for this step is the following. The nine-gauge array lies in the y-direction, and the data from its determine $|\nu_a|$ and $|\nu_b|$. If the array were rotated slightly in the (x, y)-plane, then the gauges would record slightly larger y-wavelengths for waves coming from one side, and slightly smaller y-wavelengths for waves coming from the other. By comparing the values of $|\nu_a|$ and $|\nu_b|$ obtained from the original and the rotated gauge-arrays, one could determine whether the associated waves came from the left or the right; i.e. one could determine the signs of ν_a and ν_b.

We do not actually move the gauges to obtain the second data set, but we achieve approximately the same effect by processing data from successive gauges at successively later times. Specifically, instead of using the data from all nine gauges at the same time T_0, we use the data from the jth gauge that was recorded at time

$$T_j = T_0 + (j-1)\,\Delta T,$$

where ΔT is the time between successive measurements. ($\Delta T = 0.04$ s for the 25 Hz sampling rate used in these experiments.) These data correspond approximately to data taken from a linear gauge-array whose orientation in the (x, y)-plane is rotated from the y-axis through an angle

$$\beta = \tan^{-1}[(gh)^{1/2}\,\Delta T/\Delta Y\,], \tag{B 3}$$

where ΔY is the spacing between gauges. In these experiments, $\Delta Y = 2$ m, so $\beta = 0.028$ rad ($\beta = 1.6°$). With the data rearranged in this way, we repeat step 2 to obtain $|\nu_i^+|$ and $|\nu_j^+|$. The same procedure based on $(-\Delta T)$ yields $|\nu_i^-|$ and $|\nu_j^-|$. From all of these, one can identify $\{|\nu_a^-|, |\nu_a^+|\}$ and $\{|\nu_b^-|, |\nu_b^+|\}$, because

$$|\nu_a| - |\nu_a^+| \approx |\nu_a^-| - |\nu_a|, \quad |\nu_b| - |\nu_b^+| \approx |\nu_b^-| - |\nu_b|. \tag{B 4a, b}$$

The direction of effective rotation (β) is known, so knowing whether $\{|\nu_a^-| < |\nu_a| < |\nu_a^+|\}$ or $\{|\nu_a^-| > |\nu_a| > |\nu_a^+|\}$ determines the sign of ν_a; one also finds the sign of ν_b in this way. (*Note*: If $|\nu_a|$ is small enough, then $\{\nu_a^+, \nu_a, \nu_a^-\}$ are not all of the same sign, and no combination of measured values satisfies (B 4). In this case, one finds that either

$$|\nu_a| + |\nu_a^+| \approx |\nu_a^-| - |\nu_a| \quad \text{or} \quad |\nu_a| - |\nu_a^+| \approx |\nu_a^-| + |\nu_a|.$$

If both $|\nu_a|$ and $|\nu_b|$ are small, then (B 4b) must be modified as well.)

The ν-values obtained in this way also provide estimates for $\{\mu_a, \mu_b\}$, based on

$$\mu_a \approx (\nu_a^+ - \nu_a \cos\beta)/\sin\beta.$$

By comparing these estimates with the values for μ_1 and μ_2 obtained in step 1, one determines $\{\mu_1, \nu_1\}$ and $\{\mu_2, \nu_2\}$.

Step 4: *Estimate* $\{b, \lambda, d\}$

Once $\{\mu_1, \mu_2, \nu_1, \nu_2\}$ are known, then the spatial structure of the wave pattern is fixed, and one can draw a period parallelogram in the (x, y)-plane. Next, one would like to choose, among all KP solutions of genus 2 with the same period parallelogram, the one that minimizes the r.m.s. error,

$$\tilde{\sigma}^2 = \iint [f(x, y, t) - u(x, y, t)]^2\,dx\,dy \Big/ \iint [u(x, y, t)]^2\,dx\,dy, \tag{B 5}$$

where $u(x, y, t)$ represents the measured data (normalized as in (2)), $f(x, y, t)$ represents a KP solution, and the integrals are taken over a period parallelogram. In step 6, we do essentially this. Unfortunately, $\tilde{\sigma}^2$ apparently has many local minima in parameter space, so that it is necessary to start the minimization routine close to the global minimum. The purpose of steps 4 and 5 is to obtain good starting values for the minimization in step 6.

Let u_{max} denote the measured maximum value of the (normalized) wave amplitude over the entire data set for an experiment, and u_{min} the measured minimum value. If the waves were exactly periodic, then the wave amplitude would attain its maximum and minimum values once within each period parallelogram. As discussed in §2, specifying $\{b, \lambda, d, \mu_1, \mu_2, \nu_2\}$ specifies a KP solution of genus 2, up to a translation. In particular, these parameters determine the maximum (f_{max}) and minimum (f_{min}) values of the solution, and they determine ν_1. Denote by $\nu_{1,KP}$ the value of ν_1 obtained from a particular KP solution, and by $\nu_{1,m}$ the value of ν_1 measured in steps 2 and 3. Step 4 is to minimize

$$E = \left(1 - \frac{\nu_{1,KP}}{\nu_{1,m}}\right)^2 + \left(1 - \frac{f_{max}}{u_{max}}\right)^2 + \left(1 - \frac{f_{min}}{u_{min}}\right)^2, \tag{B 6}$$

by varying $\{b, \lambda, d\}$, subject to (7), while holding $\{\mu_1, \mu_2, \nu_2\}$ fixed at the values obtained in steps 1–3. We do this numerically, using ODRPACK as described by Boggs *et al.* (1992).

Step 5: *Estimate* Φ_1 *and* Φ_2

The KP solution is now completely specified except for a spatial translation fixed by the phase constants Φ_1 and Φ_2. These constants could be obtained directly from an overhead photograph of the wavefield, such as those in figure 1, by making a contour plot of the KP solution with the same horizontal scales as the photograph, and then sliding one over the other until the phases match optimally. In the absence of such a photograph, we minimize a quantity like that in (B 5), by varying $\{\Phi_1, \Phi_2\}$ while holding fixed $\{b, \lambda, d, \mu_1, \mu_2, \nu_2\}$. However, we cannot integrate over the entire period parallelogram, as in (B 5), but only over the nine wave records. Using ODRPACK again, we minimize σ^2, from equation (10):

$$\sigma^2 = \sum_1^9 \int_0^L [f(x, y, t) - u(x, y, t)]^2 \, \mathrm{d}x \Big/ \sum_1^9 \int_0^L [u(x, y, t)]^2 \, \mathrm{d}x,$$

where L is a length of the wave record, and only $\{\Phi_1, \Phi_2\}$ are varied. Typically, we used $L = 20$ *s*.

Step 6: *Find final values of all eight parameters*

The final step is to minimize σ^2 again, allowing all eight parameters $\{b, \lambda, d, \mu_1, \mu_2, \nu_2; \Phi_1, \Phi_2\}$ to vary simultaneously. In this paper, therefore, the 'best' KP solution for a given experiment is defined to be the one that minimizes σ^2. (In Part 1, we used a different definition for 'best' fit of symmetric waves.) As mentioned above, σ^2 has several local minima in this larger space, but we start near what we believe to be the global minimum by starting at the values for these parameters found in steps 1–5.

Our experience has been that this six-step algorithm found the best KP solution for each of the fifteen available data sets for asymmetric waves. The results of the algorithm are discussed in §5. (It also converged to the best solution for the data from sixteen other experiments on symmetric waves. We will present these results elsewhere.)

Our justification for this algorithm is that it works: for each experiment on which we tested it, the algorithm found a best KP solution, with an acceptable error (σ). However, Boris Dubrovin has suggested another possible justification for the algorithm, as follows. (The rest of this paragraph is a series of speculations, which we hope to verify eventually.) Subject to some extra conditions like (1), the KP equation is a completely integrable Hamiltonian system, along the lines discussed by Dubrovin (1991, pp. 79–92). Every exact reduction of KP to a finite-dimensional system ought to be completely integrable as well. A KP solution of genus 2 is such a reduction, it has two phases, so it ought to correspond to an integrable Hamiltonian system with two degrees of freedom. Therefore, a specification of the general KP solution of genus 2 ought to contain two 'action'-type variables, and two 'angles'. Steps 1–3 of this algorithm specify the spatial structure, $\{\mu_1, \mu_2, \nu_1, \nu_2\}$. The other four variables $\{b, d; \Phi_1, \Phi_2\}$ describe the dynamical system. Step 4, which ignores phase information, apparently finds action-type variables $\{b, d\}$, while step 5 finds angles $\{\Phi_1, \Phi_2\}$. This argument suggests that step 4 would also work if the maximum and minimum values of the data set were replaced by two conserved integrals of the KP equation. In fact, it might work better.

REFERENCES

ABLOWITZ, M. J. & SEGUR, H. 1981 *Solitons and the Inverse Scattering Transform*, SIAM.

ABLOWITZ, M. J. & VILLARROEL, J. 1991 *Stud. Appl. Maths* **85**, 195–213.

BOGGS, P. T., BYRD, R. H., ROGERS, J. E. & SCHNABEL, R. B. 1992 *User's Reference Guide for ODRPACK Version* 2.01. NISTIR 92-4834, US Dept of Commerce.

DUBROVIN, B. A. 1981 *Russ. Math. Surveys* **36**, 11–92.

DUBROVIN, B. A. 1991 *Geometry of Hamiltonian Evolutionary Systems* (Lectures at University of Naples), Naples: Bibliopolis.

GUCKENHEIMER, J. & HOLMES, P. 1983 *Nonlinear Oscillations, Dynamical Systems, and Bifurcation of Vector Fields*. Springer.

HAMMACK, J., SCHEFFNER, N. & SEGUR, H. 1989 *J. Fluid Mech.* **209**, 567–589.

HAMMACK, J., SCHEFFNER, N. & SEGUR, H. 1991 *J. Geophys. Res.* **96**, 4909–4914.

KADOMTSEV, B. B. & PETVIASHVILI, V. I. 1970 *Sov. Phys. Dokl.* **15**, 539–541.

KRICHEVER, I. M. 1977 *Russ Math. Surveys* **32**, 185–213.

PEREGRINE, D. H. 1983 *Ann Rev. Fluid Mech.* **15**, 149–178,

PEREGRINE, D. H. 1985 *Proc. R. Soc. Lond.* A **400**, 1–18.

PIEXOTO, M. M. 1962 *Topology* **1**, 101–120.

SCHEFFNER, N. 1988 *Misc. Pap.* CERC-88-4, Vicksburg, MS.

SEGUR, H. & FINKEL, A. 1985 *Stud. Appl. Maths.* **73**, 183–220.

STOKES, G. G. 1847 *Trans. Camb. Phil. Soc.* **8**, pp. 441–455 (see also *Scientific Papers*, vol. **1**, pp. 197–219, Cambridge University Press).

WIEGEL, R. L. 1960 *J. Fluid Mech.* **7**, 273–286.